Biochemical and Biophysical Research Communications 435 (2013) 740–744

Contents lists available at SciVerse ScienceDirect

Biochemical and Biophysical Research Communications

journal homepage: www.elsevier.com/locate/ybbrc

Visualizing the elusive open shape of G-actin in solution by SAXS data analysis

Amin Sagar, Nagesh Peddada, Ashish k. Solanki, Vikas Choudhary, Renu Garg, Ashish *

CSIR-Institute of Microbial Technology, Chandigarh, India

ARTICLE INFO

Article history:
Received 9 May 2013
Available online 23 May 2013

Keywords:
Actin
Small angle X-ray scattering
ATP hydrolysis
Shape change

ABSTRACT

Though biochemical data upholds that ATP hydrolysis induces an opening of the nucleotide binding cleft, crystal structures of the G-actin in the absence of profillin represent the closed structure, regardless of the bound ATP/ADP. Analysis of small angle X-ray scattering (SAXS) intensities confirmed that ATP hydrolysis increases the radius of gyration (R_G) and maximum linear dimension (D_{max}) of G-actin molecules from 22.3 to 23.7 Å and 70 to 78 Å, respectively. Kratky analysis confirmed that G-actin molecules behave like globular scattering particles regardless of the bound nucleotide state. Shape reconstruction using dummy residues and inertial axes overlay with known crystal structures confirmed that the ATP or AMP-PNP bound G-actin adopts a compact shape, and the nucleotide binding site opens up with ATP hydrolysis. Importantly, our ADP-state model resembled the open shape seen for β-actin and hexokinase.

1. Introduction

Actin is a highly conserved, multifunctional protein and is essential for a vast number of processes in a cell including cell division, cell motility, cell signaling, intracellular organelle trafficking, *etc.* [17]. Actin can exist in monomeric or globular (G-actin) and in associated or filamentous form (F-actin). The dynamic equilibrium between G- and F-actin forms the basis of the remodeling/maintenance of the cytoskeleton by the eukaryotic cells [13]. The conformation of the nucleotide binding cleft of G-actin remains debatable. The reason is that the nucleotide binding pocket has been refined in closed conformation in all the crystal structures of G-actin irrespective of the phosphorylation state of the nucleotide, except the crystal structure of β-G-actin bound to profillin [4]. These observations contradict the biochemical data that supports nucleotide hydrolysis accompanied conformational changes in G-actin, similar to the changes seen in the structures of hexokinase, glyceraldehydes-3-phosphate dehydrogenase (GAPDH) and alcohol dehydrogenase (ADH) which have ATP-binding folds similar to actin. [4]. Based on crystallographic and biochemical studies, each of these proteins has two major domains which have been speculated to undergo large-scale shift in their position relative to each other upon ligand binding [7]. Despite these expectations, the open state of G-actin has been seen only in the case of β-actin bound to profillin, where the subdomains 2 and 4 are away from each other, thus making the nucleotide binding cleft between them distinctly accessible to bulk solvent [4,23]. Earlier studies based on partial enzymatic digestion [19,14] support that the molecule is significantly more susceptible to cleavage in the ADP state compared to the ATP state, implying a more open conformation [4]. Yet, this structure never established that the actin can adapt an open shape on its own.

The closed conformation of actin in all but one of the crystals may be because of two reasons. Firstly, the small difference in the free-energy of the open and closed conformations may render the nucleotide binding cleft susceptible to the forces of crystal packing, thereby favoring the closed conformation [15]. Secondly, the presence of the different crosslinking agents and/or bound proteins may disrupt the γ-phosphate sensing mechanism so that the conformation of the nucleotide binding cleft becomes insensitive to the phosphorylation state of the nucleotide [8]. Earlier, it has been suggested that the subdomain movements affect signal transduction across different parts of the actin molecule [5]. Overall, we feel that a holistic understanding of the effect of phosphorylation state of the bound nucleotide on the shape of actin is crucial to understand the biophysical properties of G-actin (as well as F-actin). For G-actin, an unequivocal evidence for the opening of the nucleotide cleft will provide a plausible explanation for the differential binding affinities of a number of proteins including profillin, thymosin beta 4 and actin-depolymerization factor for the G- and F-forms of actin [2,11,3]. For F-actin, open *vs.* close shapes may provide a template structure of an F-actin protomer which reliably fits in the electron microscopy models of ADP-F-actin [1]. Here, we report SAXS data analysis and structures restored for muscle G-actin bound to non-hydrolyzable ATP analog, AMP-PNP and at multiple time points during the course

* Corresponding author. Address: CSIR-Institute of Microbial Technology, Sector 39-A, Chandigarh 160036, India. Fax: +91 1722690585.
E-mail address: ashgang@imtech.res.in (Ashish).

0006-291X/$ - see front matter © 2013 Elsevier Inc. All rights reserved.
http://dx.doi.org/10.1016/j.bbrc.2013.05.055

of hydrolysis of ATP to ADP. Overcoming the need for a diffractable single crystal or a monophasic system essential for NMR based studies, our SAXS data analysis and modelling show that G-actin undergoes a distinct conformational change upon the hydrolysis of ATP to ADP. Our results clearly show that ADP-bound G-actin adopts a solution shape which is much more open and resembles the proposed hexokinase-like shape.

2. Materials and methods

2.1. Actin extraction from chicken muscle

Actin was extracted from chicken breast muscle by employing the protocol detailed by Spudich and coworkers with minor modifications [18]. Briefly, actin was solubilized by suspending the acetone muscle powder in pre-chilled G-buffer (0.2 mM Tris, 0.2 mM $CaCl_2$, 0.2 mM ATP, 0.5 mM 2-mercaptoethanol, pH 8) at 4 °C. Polymerization of the actin was induced by the addition of 50 mM KCl and 2 mM $MgCl_2$ at room temperature for 2 h followed by addition of solid KCl with continuous stirring at 4 °C to the final concentration of 0.8 M. Polymerized actin was collected by the ultra centrifugation at 40,000*g* for 2.5 h at 4 °C and the pellet was thoroughly washed and softened by overnight incubation in G-buffer. The softened pellet was homogenized thoroughly and kept for extensive dialysis against G-buffer for 3 days with buffer exchange containing fresh aliquot of ATP at every 24 h. Finally, G-actin was obtained by centrifugation at 40,000*g* for 2 h and concentration was determined by measuring the optical density at 290 nm (OD 290 nm∼0.62, 1 mg/ml). Purity of the G-actin samples was affirmed by presence of a single band close to 40 KDa in SDS-PAGE (8% cross-linking). Protein concentration during data collection was re-estimated using observed intensities for standard samples. Particle size determination of monomeric actin was done by measuring diffusion coefficient values using a Dynamic Light Scattering (DLS) instrument (DelsaNano C, Beckman Coulter).

2.2. Synchrotron SAXS data acquisition and analysis

The dialysis buffer for G-actin was changed every 24 h with fresh ATP. 12 h prior to SAXS experiments, G-actin was distributed in three parts. One part was dialyzed against G-buffer containing AMP-NP (with two changes), second part was dialyzed with buffer containing fresh ATP (with two changes) and third part was left as such. These experiments were carried out using AMICON dialysis cassettes and at 4 °C. SAXS data were collected at different time points from G-actin dialyzed against AMP-NP and ATP buffers (and the dialysis buffer). All SAXS data were acquired at X9 beam line in National Synchrotron Light Source (Brookhaven National Laboratory, NY) and analyzed as described previously [6]. For each individual experiment, 200 μl of protein solution and matched buffer were exposed to X-rays for 60 s at a flow rate of ∼50 μL/min (three runs). The scattering images were collected on Pilatus detectors. The beam centre and the distance between the sample and the detector was determined using scattering data from silver behenate powder. The transmission counts at the beam stopper were used to scale the images. Circular averaging was done for both protein solutions and buffers, and then buffer contributions were subtracted to obtain one dimensional scattering intensity profile [*I(Q)*] of the protein molecules as a function of Q, where Q is defined as $4\pi\sin\theta/\lambda$. The *I(Q)* profiles were analyzed by PRIMUS [9] and GNOM [20] programs to calculate shape parameters by Guinier approximations and Indirect Fourier transformations, respectively. During Guinier approximations, only low Q data points satisfying the relationship that $Q \cdot R_G^2 \leqslant 1.3$ were considered. Additionally, probability of finding intraparticle vectors equal to 0 Å and D_{max} of scattering particle were considered to be zero during indirect Fourier transformation.

2.3. Structure reconstruction within SAXS I(Q) profiles

To visualize the ATP hydrolysis accompanied changes in the shape of G-actin, uniform density modeling approach was employed using DAMMINIQ software [21]. Using acquired SAXS data as reference, ten models were generated for G-actin bound to ATP, ATP/ADP and ADP considering no shape and symmetry bias. Individual solutions were averaged using DAMAVER suite of programs to obtain predominant scattering shape of the nucleotide bound G-actin in solution [22]. Using SUPCOMB program, the inertial axes of the resultant low resolution shapes for G-actin at different time points and known structures from X-ray diffraction were superimposed [10]. Open-source programs SPDB viewer and PyMOL were used for graphical analysis, and figure generation. Data plotting and curve-fitting was done using OriginLab software.

3. Results

3.1. SAXS based tracking of shape changes accompanying ATP hydrolysis

The critical concentration of G-actin for polymerization has been shown to be dependent on ionic strength and phosphorylation state of the nucleotide. Moreover, ATP-G-actin has ∼24 times lower critical concentration than ADP-G-actin. Also, ionic strength of the buffer has been shown to significantly alter the polymerization dynamics with higher concentrations of $MgCl_2$ favoring the polymerization [12]. To study actin in its non-associated or G-form, we deliberately kept the protein at low concentration (∼0.5 mg/ml), in low ionic strength buffer, and replenished fresh ATP containing buffer at every 24 h. DLS experiments estimated the hydrodynamic radii of ∼3.8–4.0 nm for actin molecules in solution suggesting that the protein molecules remained monomeric under these conditions. Further, profiles of the acquired SAXS *I(Q)* support monodisperse nature of scattering particles in solution during data collection (Fig. 1A). To track the shape changes in the actin molecule accompanying ATP hydrolysis, SAXS data were collected from G-actin samples dialyzed against G-buffer containing fresh ATP and AMP-PNP at different time-points (*scattering I(Q) profiles of only three samples are presented here;* Fig. 1).

Peak-like profiles of the Kratky plots confirmed that the G-actin protein molecules possess globular scattering nature irrespective of the phosphorylation state of the nucleotide (Fig. 1A and inset). Decreasing Q-range and slopes of the allowed linear fit zone in the Guinier analysis of these datasets brought forth that R_G of the protein increases with ATP hydrolysis (Fig. 1B). Indirect Fourier transformation of the *I(Q)* data provided the pairwise distance distribution function [*P(r)*] for the scattering shapes of G-actin. In agreement with the Guinier analyses, *P(r)* curves indicated that the D_{max} and R_G of the G-actin molecules increase from 70 to 78 Å, and from 22.4 to 23.7 Å, respectively as the bound ATP was hydrolyzed (Fig. 1C and Table 1). Data analysis showed that R_G of the G-actin gradually increased from 22.4 Å (∼5 min) to reach maximum observed value of ∼23.7 Å by 6 h. Based on this curve, the half-time of ATP hydrolysis under these conditions is about 2.5 h. Importantly, this observation is in correlation with hydrolysis time-spans reported earlier based on fluorescence based experiments [16]. Alongside, SAXS data was acquired from G-actin dialyzed against AMP-PNP buffer at different time points and never dialyzed with ATP (Fig. 1D). The estimated R_G values from indirect Fourier transformation of these datasets showed that the shape parameters of G-actin bound to non-hydrolyzable nucleotide (AMP-PNP) do not vary. Throughout the time-span studied, the

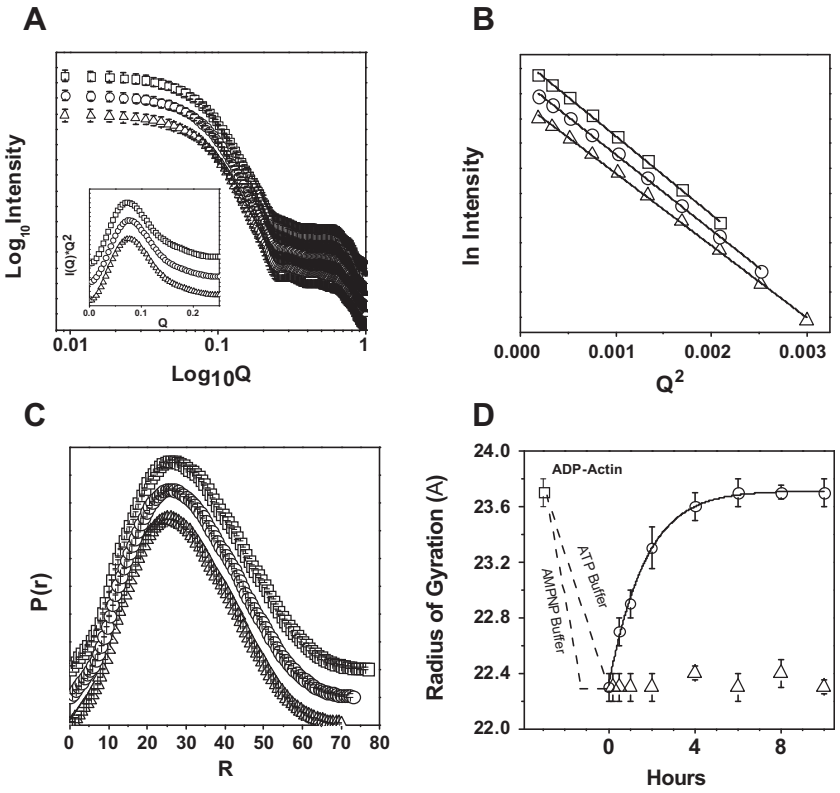

Fig. 1. SAXS data analysis for G-actin in ATP buffer after 5 min (○), 2 h (△) and 8 h (□) of last exchange are presented here. (A) SAXS intensity *I(Q)* data, inset shows their Kratky profiles (B) Linear regions of the Guinier approximations, and (C) *P(r)* curves computed from indirect Fourier transformation of the measured SAXS data.

Table 1
Shape parameters of the protein molecules deduced from analyzing the SAXS datasets are tabulated below.

Protein	Indirect Fourier Transformation			Kratky analysis	Estimated conc. (mg/ml)
	D_{max} (Å)	R_G (Å)	Estimated I_0		
Lysozyme (14.2 KDa) (concentration series)	44	14.2	28	Globular	1[a]
G-actin (42 KDa)					
ATP Buffer					
~5 min	70	22.3 ± 0.1	41.4	Globular	0.5
0.5 h	72	22.7 ± 0.1	41.3	Globular	0.5
1 h	74	22.9 ± 0.1	40.6	Globular	0.49
2 h	76	23.3 ± 0.15	41.4	Globular	0.5
4 h	78	23.6 ± 0.1	39.8	Globular	0.48
6 h	78	23.7 ± 0.1	40.7	Globular	0.49
8 h	78	23.7 ± 0.05	41.2	Globular	0.5
10 h	78	23.7 ± 0.1	40.8	Globular	0.5
AMP-PNP Buffer					
~5 min	70	22.3 ± 0.1	40.6	Globular	0.49
0.5 h	70	22.3 ± 0.1	39.8	Globular	0.48
1 h	70	22.3 ± 0.1	39.8	Globular	0.48
2 h	70	22.3 ± 0.1	40.6	Globular	0.49
4 h	72	22.4 ± 0.05	41.4	Globular	0.5
6 h	70	22.3 ± 0.1	40.6	Globular	0.49
8 h	72	22.3 ± 0.1	39.8	Globular	0.48
10 h	70	22.4 ± 0.05	41.4	Globular	0.5
ADP State	78	23.7 ± 0.1	40.6	Globular	0.49

[a] Estimated for 1 mg/ml of lysozyme from a predetermined concentration series of lysozyme (having five samples from 0.7–3.7 mg/ml).

D_{max} and R_G of the AMP-PNP-bound G-actin remained close to 70 and 22.3–22.4 Å, respectively. Moreover, comparable dimensions (D_{max} and R_G close to 78 and 23.6–23.7 Å, respectively) of ADP-bound G-actin (*the sample which was not hydrolyzed against ATP or after hydrolysis of ATP in solution*) indicated that the nucleotide hydrolysis accompanied shape changes in G-actin are reversible (Fig. 1D and Table 1).

Observed I_0 values from samples of G-actin bound to different nucleotides (ADP/ATP/AMP-PNP) supported that protein concentrations were comparable during SAXS data acquisitions and observed shape changes are induced by nucleotide hydrolysis only (Table 1). Our data suggested that ATP-bound G-actin adopts a tighter shape which slowly opens as bound ATP gets hydrolyzed and phosphate ion is released leading to formation of ADP-bound

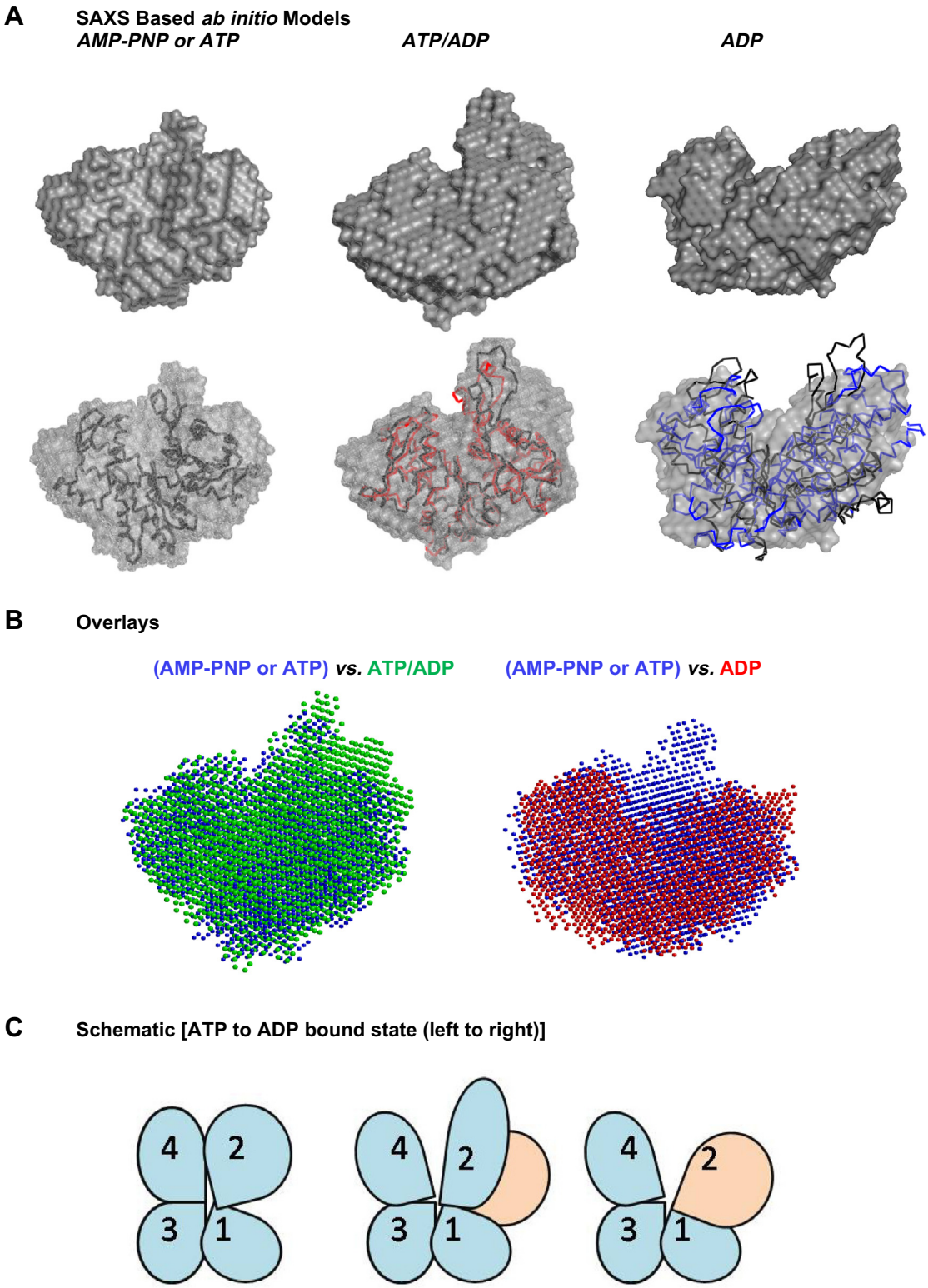

Fig. 2. (A) SAXS data based averaged models of G-actin bound to different states of nucleotides. (*Left*) The AMPNP or ATP model (gray) is overlaid with crystal structure of G-actin with AMPNP (PDB ID: 1NWK, black trace). (*Middle*) Two crystal structures of G-actin: bound to ADP (PDB ID: 1J6Z, red trace) and bound to profillin (PDB ID: 1HLU, black trace) have been aligned within volume of SAXS data based model of ATP/ADP actin (gray). (*Right*) The crystal structures of actin only (from profillin bound state, PDB ID: 1HLU, black trace) and hexokinase (PDB ID: 1IG8, blue trace) have been overlaid with SAXS data based model (gray). (B) Different SAXS data based models have been overlaid by alignment of inertial axes to compare the extent of shape change. (C) Schematic summarizes the changes in relative positioning of the subdomains of G-actin as a function of bound-ATP hydrolysis. (For interpretation of the references to colour in this figure legend, the reader is referred to the web version of this article.)

G-actin. Since ATP hydrolysis starts at zero time point, compact shape of ATP-bound G-actin was supported by the shape parameters seen for AMP-PNP-bound G-actin. In our experiments, datasets from sample with ATP at different time points represent average scattering shape of G-actin molecules bound to ATP as well as ADP. At extended time points (6, 8 and 10 h), when most of the

ATP is hydrolyzed, the ADP-bound G-actin showed a much opened shape. Calculated χ^2 values between SAXS *I(Q)* profiles of G-actin in ATP buffer at ~5 min. and SAXS *I(Q)* profiles of G-actin in AMP-PNP buffer at any given time was only 1.1–1.2. Similarly, the χ^2 value between G-actin in ATP buffer for 8 (or 10) h and SAXS *I(Q)* profile from sample in ADP (not dialyzed against ATP) was 1.1. These similarities in *I(Q)* profiles supported that G-actin in fresh ATP is similar to that bound to AMP-PNP. Importantly, singular value decomposition (SVD) of the SAXS datasets yielded that the ATP-hydrolysis associated shape change in G-actin molecule is a two-state process.

4. Discussion

4.1. Visualizing nucleotide hydrolysis induced opening of G-actin

We modeled the "closed" state of G-actin by using acquired SAXS datasets of G-actin in fresh ATP and AMP-PNP buffer (Fig. 2). Alongside, the SAXS datasets from G-actin in ADP buffer and ATP buffer (8 h after exchange) were used to model the "open" state of G-actin. To visualize the intermediate shape, the SAXS dataset of G-actin in ATP buffer for 2 h was used. Overlay of these models with known crystal structures clearly demonstrated that nucleotide state induced shape changes are primarily in the nucleotide binding portion of G-actin structure. The averaged *abinitio* model for G-actin in ATP/AMP-PNP state shows a compact shape with virtually no cleft visible. Further, the model for ATP/ADP-actin shows a slightly open shape with a clearly visible cleft. In sharp contrast, the model for ADP-actin shows a radically different shape with a large cleft clearly indicating an opening of the nucleotide binding cleft of actin upon the hydrolysis of ATP to ADP. Importantly, the SAXS based closed model of actin closely resembles the closed structure of AMP-PNP-bound actin (PDB ID: 1NWK) (CRYSOL program computed a χ^2 value of 1.0). It is pertinent to mention here that in the AMP-PNP-bound crystal structure, crucial 11 residues (40–51) in DB-loop of actin could not be resolved. Interestingly, these residues have been suggested to be disordered in ATP-bound state and α-helical in ADP-bound crystal structure (PDB ID: 1J6Z). Our model of ATP/ADP-actin can actually accommodate both the crystal structures of G-actin, the partly closed ADP-structure of actin (PDB ID: 1J6Z) and the open structure of β-G-actin in the profillin bound structure (PDB ID: 1HLU). This observation is consistent with the fact that our ATP/ADP-model was generated from sample of G-actin in ATP buffer for 2 h, and considering the half time of ATP hydrolysis is about 2.5 h, we have modeled a shape which is an average of closed (ATP) as well as open (ADP) state (Fig. 2B). The significantly open model of ADP-G-actin compared better with the structure of β-actin bound to profillin (PDB ID: 1HLU) than with the crystal structure of ADP-bound G-actin (PDB ID: 1J6Z). Additionally, CRYSOL program computed χ^2 values of 1.5 and 1.9 between the acquired SAXS *I(Q)* profile from ADP-G-actin and crystal structures of profillin bound G-actin and ADP-G-actin, respectively. Earlier investigators have suggested different domains of G-actin to undergo changes in their relative positions in space similar to those seen for hexokinase, GAPDH and ADH [4]. Thus, we compared our open model of ADP-G-actin with the nucleotide binding portion of hexokinase and found that our open model matched even better with the fold depicted by hexokinase (PDB ID: 1IG8 and χ^2 value 1.4). Overall, our models showing closed to open shape of G-actin provide direct structural evidence that the open structure seen for β-actin (bound to profillin) is accessible to α-actin as well and that too in its unliganded form. Our results support that additional to conformational change across DB loop, subdomains of G-actin undergo significant shift in their relative positioning as a result of bound nucleotide hydrolysis (Fig. 2C).

Acknowledgments

This work has been supported by the funds from CSIR-INDIA (OLP-0056) and CSIR network project "UNSEEN" and "BUGS TO DRUGS". RG is a recipient of DST-WOSA (SR/WOS-A/LS-106/2009). AS, NP and AKS are recipients of DBT and CSIR Research Fellowships. Use of National Synchrotron Light Source, Brookhaven National Laboratory, was supported by the U.S. Department of Energy, Office of Science, Office of Basic Energy Sciences, under Contract No. DEAC02-98CH10886. Authors acknowledge the consistent support from Faculty and Staff of IMTECH. This is IMTech communication number 002/2013.

References

[1] L.D. Belmont, A. Orlova, et al., A change in actin conformation associated with filament instability after P-i release, Proc. Nat. Acad. Sci. USA 96 (1) (1999) 29–34.
[2] M.F. Carlier, C. Jean, et al., Modulation of the interaction between G-actin and Thymosin-Beta-4 by the Atp Adp Ratio - possible implication in the regulation of actin dynamics, Proc. Nat. Acad. Sci. USA 90 (11) (1993) 5034–5038.
[3] M.F. Carlier, V. Laurent, et al., Actin depolymerizing factor (ADF/cofilin) enhances the rate of filament turnover: implication in actin-based motility, J. Cell Biol. 136 (6) (1997) 1307–1322.
[4] J.K. Chik, U. Lindberg, et al., The structure of an open state of beta-actin at 2.65 angstrom resolution, J. Mol. Biol. 263 (4) (1996) 607–623.
[5] R.H. Crosbie, C. Miller, et al., Structural connectivity in actin: effect of C-terminal modifications on the properties of actin, Biophys. J. 67 (5) (1994) 1957–1964.
[6] R. Garg, N. Peddada, et al., Visual insight into how low pH alone can induce actin-severing ability in gelsolin under calcium-free conditions, J. Biol. Chem. 286 (23) (2011) 20387–20397.
[7] M. Gerstein, A.M. Lesk, et al., Structural mechanisms for domain movements in proteins, Biochemistry 33 (22) (1994) 6739–6749.
[8] W. Kabsch, H.G. Mannherz, et al., Atomic-structure of the actin - Dnase-I complex, Nature 347 (6288) (1990) 37–44.
[9] P.V. Konarev, V.V. Volkov, et al., PRIMUS: a Windows PC-based system for small-angle scattering data analysis, J. Appl. Crystallogr. 36 (2003) 1277–1282.
[10] M.B. Kozin, D.I. Svergun, Automated matching of high- and low-resolution structural models, J. Appl. Crystallogr. 34 (2001) 33–41.
[11] D. Pantaloni, M.F. Carlier, How profilin promotes actin filament assembly in the presence of Thymosin-Beta-4, Cell 75 (5) (1993) 1007–1014.
[12] D. Pantaloni, M.F. Carlier, et al., The critical concentration of actin in the presence of ATP increases with the number concentration of filaments and approaches the critical concentration of actin.ADP, J. Biol. Chem. 259 (10) (1984) 6274–6283.
[13] T.D. Pollard, L. Blanchoin, et al., Molecular mechanisms controlling actin filament dynamics in nonmuscle cells, Annu. Rev. Biophys. Biomol. Struct. 29 (2000) 545–576.
[14] M.A. Rould, Q. Wan, et al., Crystal structures of expressed non-polymerizable monomeric actin in the ADP and ATP states, J. Biol. Chem. 281 (42) (2006) 31909–31919.
[15] E.P. Sablin, J.F. Dawson, et al., How does ATP hydrolysis control actin's associations?, Proc Nat. Acad. Sci. USA 99 (17) (2002) 10945–10947.
[16] L.A. Selden, L.C. Gershman, et al., Conversion of ATP-actin to ADP-actin reverses the affinity of monomeric actin for Ca^{2+} vs Mg^{2+}, FEBS Lett. 217 (1) (1987) 89–93.
[17] P. Sheterline, J. Clayton, et al., Actin, Protein Profile 2 (1) (1995) 1–103.
[18] J.A. Spudich, S. Watt, The regulation of rabbit skeletal muscle contraction. I. biochemical studies of the interaction of the tropomyosin-troponin complex with actin and the proteolytic fragments of myosin, J. Biol. Chem. 246 (15) (1971) 4866–4871.
[19] H. Strzelecka-Golaszewska, J. Moraczewska, et al., Localization of the tightly bound divalent-cation-dependent and nucleotide-dependent conformation changes in G-actin using limited proteolytic digestion, Eur. J. Biochem. 211 (3) (1993) 731–742.
[20] D.I. Svergun, Determination of the regularization parameter in Indirect-transform methods using perceptual criteria, J. Appl. Crystallogr. 25 (1992) 495–503.
[21] D.I. Svergun, M.V. Petoukhov, et al., Determination of domain structure of proteins from X-ray solution scattering, Biophys. J. 80 (6) (2001) 2946–2953.
[22] V.V. Volkov, D.I. Svergun, Uniqueness of ab initio shape determination in small-angle scattering, J. Appl. Crystallogr. 36 (2003) 860–864.
[23] W. Wriggers, K. Schulten, Stability and dynamics of G-actin: back-door water diffusion and behavior of a subdomain 3/4 loop, Biophys. J. 73 (2) (1997) 624–639.